

# Journal of Biomedical Optics

[SPIEDigitalLibrary.org/jbo](http://SPIEDigitalLibrary.org/jbo)

## **Calcium influx affects intracellular transport and membrane repair following nanosecond pulsed electric field exposure**

Gary Lee Thompson  
Caleb C. Roth  
Danielle R. Dalzell  
Marjorie Kuipers  
Bennett L. Ibey

# Calcium influx affects intracellular transport and membrane repair following nanosecond pulsed electric field exposure

Gary Lee Thompson,<sup>a,\*</sup> Caleb C. Roth,<sup>b</sup> Danielle R. Dalzell,<sup>c</sup> Marjorie Kuipers,<sup>c</sup> and Bennett L. Ibey<sup>c</sup>

<sup>a</sup>Oak Ridge Institute for Science and Education, JBSA Fort Sam Houston, Texas 78234

<sup>b</sup>University of Texas Health Science Center at San Antonio, Department of Radiological Sciences, San Antonio, Texas 78229

<sup>c</sup>711th Human Performance Wing, JBSA Fort Sam Houston, Texas 78234

**Abstract.** The cellular response to subtle membrane damage following exposure to nanosecond pulsed electric fields (nsPEF) is not well understood. Recent work has shown that when cells are exposed to nsPEF, ion permeable nanopores (<2 nm) are created in the plasma membrane in contrast to larger diameter pores (>2 nm) created by longer micro- and millisecond duration pulses. Nanoporation of the plasma membrane by nsPEF has been shown to cause a transient increase in intracellular calcium concentration within milliseconds after exposure. Our research objective is to determine the impact of nsPEF on calcium-dependent structural and repair systems in mammalian cells. Chinese hamster ovary (CHO-K1) cells were exposed in the presence and absence of calcium ions in the outside buffer to either 1 or 20, 600-ns duration electrical pulses at 16.2 kV/cm, and pore size was determined using propidium iodide and calcium green. Membrane organization was observed with morphological changes and increases in FM1-43 fluorescence. Migration of lysosomes, implicated in membrane repair, was followed using confocal microscopy of red fluorescent protein-tagged LAMP1. Microtubule structure was imaged using mEmerald-tubulin. We found that at high 600-ns PEF dosage, calcium-induced membrane restructuring and microtubule depolymerization coincide with interruption of membrane repair via lysosomal exocytosis. © 2014 Society of Photo-Optical Instrumentation Engineers (SPIE) [DOI: 10.1117/1.JBO.19.5.055005]

Keywords: nanosecond pulsed electric fields; lysosomal exocytosis; cytoskeleton; FM1-43; nanopores.

Paper 140081PR received Feb. 9, 2014; revised manuscript received Mar. 28, 2014; accepted for publication Apr. 8, 2014; published online May 13, 2014.

## 1 Introduction

Nanosecond pulsed electric fields (nsPEF) have been studied for applications ranging from killing cancer cells to food sterilization to electromuscular incapacitation.<sup>1-9</sup> Exposure of mammalian cells to high voltage nanosecond duration electrical pulses has been shown to produce various effects including the permeabilization of intracellular granules<sup>10</sup> and plasma membrane,<sup>11,12</sup> phosphatidylserine translocation,<sup>13,14</sup> intracellular calcium bursts,<sup>15</sup> and necrotic or apoptotic cell death.<sup>16-20</sup> These effects appear different from those observed after micro- and millisecond duration exposures that produce large pores in the plasma membrane capable of allowing transfer of large molecules into the cytoplasm.<sup>21</sup> Theoretical simulations predict that nanosecond electric pulses cause ultraporations throughout the cellular volume in contrast to longer pulses that predominantly impact the plasma membrane.<sup>22,23</sup> While the effects attributed to nsPEF are well demonstrated, how cells repair membrane disruptions following exposure to nsPEF, and whether these repair mechanism(s) differ from longer pulse exposures, remains unknown.

Plasma membrane repair is an essential mechanism of mammalian cells for survival. For small disruptions, plasma membranes have been shown to “self-seal” due to thermal energy and changes in the membrane conformation (movement of phospholipids from the inside to the outside of the membrane).<sup>21</sup> Self-sealing has been shown to occur in both the presence

and absence of extracellular calcium. Active membrane repair by exocytosis of intracellular vesicles has been seen with large disruption to the plasma membrane by microinjection pipettes and has been shown to be dependent on the influx of extracellular Ca<sup>2+</sup>.<sup>24</sup> Previous studies have shown that plasma membrane resealing is regulated by the delivery of intracellular membranes to the compromised site, by a mechanism resembling Ca<sup>2+</sup>-regulated exocytosis<sup>25</sup> and phagocytosis.<sup>26</sup> Recent studies have shown that the Ca<sup>2+</sup>-regulated secretory vesicles correspond to lysosomes.<sup>27-29</sup> Rodriguez et al. showed that the conventional lysosomes can be induced to fuse with the plasma membrane.<sup>30</sup> Lysosomes were once thought only to serve as the “garbage disposal” of the cell containing acid hydrolase enzymes in order to break down waste and cellular debris. Continuing research, however, shows that lysosomes may serve a much higher purpose in the cell as an active participant in the plasma membrane repair by adding their membrane to fill holes in the plasma membrane.

Cytoskeletal integrity is integral to membrane repair by lysosomal exocytosis. Interaction of lysosome vesicles with the plasma membrane is regulated by coordination between local Ca<sup>2+</sup> concentrations and cortical F-actin, which capture vesicles then depolymerizes to allow passage and fusion of the vesicles to the membrane.<sup>31-33</sup> Prior to arrival at the actin cortex, lysosome translocation across the cytoplasm is directed by the microtubule network,<sup>34-36</sup> evidenced by disruption with the microtubule antagonist, nocodazole. Antagonists of actin and

\*Address all correspondence to: Gary L. Thompson, E-mail: [gary.l.thompson205.ctr@mail.mil](mailto:gary.l.thompson205.ctr@mail.mil)

intermediate filament did not affect lysosome movement. Locomotion of lysosomes along microtubules is attributable to kinesin<sup>37,38</sup> or kinesin-like<sup>39</sup> molecular motors in a nucleotide triphosphate-dependent manner.

Calcium concentrations also impact this cytoplasmic translocation of lysosomes by modulating microtubule polymerization and depolymerization. *In vitro*, polymerization of isolated tubulin at 35°C is blocked in solutions containing 6  $\mu\text{M}$   $\text{Ca}^{2+}$ ,<sup>40</sup> and induction of fragmentation or depolymerization is observed beginning around 1 or 100  $\mu\text{M}$  external  $\text{Ca}^{2+}$ , respectively.<sup>41–43</sup> *In vivo*, similar levels of external  $\text{Ca}^{2+}$  elicit similar effects on microtubules, with calmodulin shifting the effective  $\text{Ca}^{2+}$  concentrations downward and microtubule-associated proteins shifting it upward.<sup>41,44,45</sup> It should be noted that the localized  $\text{Ca}^{2+}$  concentrations within the cell are expected to be higher than external concentrations, and diffusion of  $\text{Ca}^{2+}$  through the cytoplasm produces a pattern of microtubule disassembly from the periphery to center of the cell.<sup>41</sup>

Electroporation effects on the tubulin cytoskeleton have been observed to be calcium-dependent. Harkin and Hay<sup>46</sup> exposed white leghorn chick embryo corneal fibroblasts grown in collagen gels (Type I from rat tail) to a milliseconds' duration, exponentially decaying pulse of 750 V/cm and 960  $\mu\text{F}$ . They found that if exposed in culture medium (containing  $\sim 1$  mM  $\text{Ca}^{2+}$ ),  $\geq 75\%$  of the cells displayed only a few microtubules. Many more microtubules were observed in cells exposed within calcium-free, intracellular electroporation buffer (ICEB). Furthermore, the addition of calcium chloride at  $\geq 100$  mM to ICEB led to microtubule disruption upon exposure. Kanthou et al.<sup>47</sup> have also reported disruption of microtubules in endothelial cells supported on microporous filter inserts upon exposure to three square wave electroporation pulses at 1 Hz of 50 to 200 V/cm and 100  $\mu\text{s}$  duration, although no experiments controlling  $\text{Ca}^{2+}$  concentrations were performed. These studies point toward the significant role of calcium in cellular signaling, structural and repair responses within the initial seconds and minutes following nsPEF exposure.

The goal of this study is to investigate the impact of calcium on cell response to the plasma membrane permeabilization by nsPEF exposure, specifically in terms of intracellular transport and membrane repair. Previous studies have shown that the membrane damage elicited by milli- and microsecond electric pulses can induce lysosomal exocytosis as evident by positive expression of LAMP-1 on the surface of the plasma membrane,<sup>48</sup> and others have demonstrated extensive microtubule disruption following such electric pulse exposure. In this study, we theoretically created large pores in the plasma membrane (detected by propidium uptake) by delivering 20 nsPEF and formed predominant nanopores (detected by calcium green) using single-pulse exposures. We measured the plasma membrane response to both exposures by monitoring the rearrangement of the plasma membrane, the stability of microtubules, and the movement of lysosomes.

## 2 Materials and Methods

### 2.1 Cell Lines and Reagents

CHO-K1 cells and media components were acquired from American Type Culture Collection (ATCC, Manassas, VA). Cells were grown in 75-cm<sup>2</sup> flasks at 37°C with 5% CO<sub>2</sub> in air. CHO-K1 cells were propagated in Ham's F12K medium supplemented with 10% FBS and 1% penicillin/streptomycin.

For transfection of red fluorescent protein-lysosomal-associated membrane protein 1 (RFP-LAMP1) and mEmerald-tubulin into CHO-K1 cells, an Effectene kit (Qiagen, Gaithersburg, MD, #301425) was used, and the line was maintained using G418 (Calbiochem, Philadelphia, PA, #345812). A custom buffer solution used throughout the experiments consisted of 2 mM MgCl<sub>2</sub>, 5 mM KCL, 10 mM 4-(2-hydroxyethyl)-1-piperazineethanesulfonic acid (HEPES), 10 mM Glucose, 2 mM CaCl<sub>2</sub>, and 135 mM NaCl (Sigma-Aldrich, St. Louis, MO). The buffer osmolality was measured and pH was adjusted to 7.4 using NaOH. In experiments where calcium was removed from the outside solution, 2 mM CaCl<sub>2</sub> was replaced by 2 mM potassium ethylene glycol tetraacetic acid (K-EGTA) (Sigma-Aldrich) added to the buffer solution. For experiments involving paclitaxel (semisynthetic from *Taxus* sp., Sigma-Aldrich, #7191), it was diluted in dimethyl sulfoxide (DMSO), added to complete growth medium at final concentrations of 1.5 nM paclitaxel and 17.6  $\mu\text{M}$  DMSO, and then introduced to cells for 2 h incubation at 37°C and 5% CO<sub>2</sub>. Cells were washed twice with custom buffer solution and imaged with the same concentration of paclitaxel in DMSO in the custom buffer as was in the complete growth medium. Custom buffer solutions containing polyethylene glycol (PEG, number average molecular weight  $M_n = 300$ , Sigma-Aldrich, #202371) were prepared as by Nesin et al.<sup>49</sup> In short, 100 mM NaCl in the above custom buffer was replaced with 152 mM PEG, so that only 35 mM NaCl was added. Osmolality of the final solution was confirmed to be between 290 and 300 mOsm with a freezing point osmometer (Advanced Instruments, Inc., Norwood, MA). Imaging was performed at room temperature, between 22°C and 24°C.

### 2.2 Cell Staining

CHO-K1 cells were trypsinized, pelleted, and resuspended in complete growth medium. Cells were counted with a Beckman Coulter Z1 particle counter (Brea, CA) and resuspended in growth medium to 1200 cells/ $\mu\text{L}$ . Approximately  $6.0 \times 10^3$  cells were plated on 35 mm glass bottom dishes coated with poly-D-lysine (#P35GC-0-10-C, MatTek Corporation, Ashland, MA) and allowed to incubate overnight. After 24 h, the cells were washed first with Dulbecco's phosphate buffered saline and then twice with the custom buffer solution (either with or without calcium). To stain cells with calcium green-1 AM ester (CaGr, #C-3011MP, Molecular Probes, Life Technologies, Eugene, OR), 2 mL buffer solution (with or without calcium) and 6  $\mu\text{L}$  CaGr were added to the dish and allowed to sit for 40 min. Cells were washed twice more with fresh buffer solution (with or without calcium) and a final 2 mL of buffer solution was added for imaging. To stain cells with propidium iodide (PI, #P4864, Sigma-Alrich), 10  $\mu\text{L}$  propidium iodide solution (1 mg/mL) was added to 2 mL of buffer solution. To stain cells with FM1-43, 2 mL buffer solution (with or without calcium) and 12.2  $\mu\text{L}$  FM1-43 (#T-3163, Molecular Probes) stock solution were added.

### 2.3 Pulsing System Setup and Dosimetry

A Zeiss 710 LSM confocal microscope (Carl Zeiss MicroImaging GmbH, Jena, Germany) with a DIC40X 1.2NA objective (Carl Zeiss MicroImaging GmbH, Germany) was used to image the CHO-K1 cells. A stimulating electrode composed of two parallel tungsten wires (100- $\mu\text{m}$  separation) was crafted in-house and mounted at a 30–35 deg angle on

an electrically controllable micromanipulator (Sutter Instruments MP252), as described in previous publications.<sup>12</sup> In brief, a digital relay generator (Stanford DG535) generates two transistor-transistor logic (TTL) pulses. The first TTL pulse is delivered to the microscope controller and begins imaging at time = 0 s. The second TTL pulse is delivered to the pulse generator (HP8112A) after a preset delay to deliver a set number of TTL pulses to the custom transmission line pulsing system. The pulsing system (Old Dominion University) can deliver six discrete pulse widths (10, 30, 60, 200, 400, or 600 ns) at a maximum repetition rate of 5 Hz. A high voltage power supply rapidly charges the pulses at voltages ranging from 0 to 999 V in 0.1 V increments, determining the pulse amplitude. A Tektronix TDS3052 500-MHz oscilloscope was connected across a 50- $\Omega$  load resistor to confirm pulse delivery for each exposure. A finite-difference time-domain model was constructed based on the electrode geometry, as in previous publications, to calculate the electric field amplitude at the cell position.<sup>50</sup> Due to inherent electric field nonuniformity near the electrodes, the cells were positioned at 50  $\mu\text{m}$  below the electrodes using the micromanipulator.

#### 2.4 Data Acquisition and Analysis

The microscope was programmed to acquire a 40X image every second for 30 s for cells containing CaGr and FM1-43. Cells with PI were imaged every 8 s for 3 min. Cells transfected with RFP-LAMP1 and mEmerald-tubulin were imaged every 3 s per  $720 \times 720$  pixels for 8 min. Cells were pulsed at a 5-s time delay for CaGr, FM1-43 and PI experiments and a 240-s time delay for RFP-LAMP1 and mEmerald-tubulin experiments with either 1 pulse (low dose) or 20 pulses (high dose). All pulses used in the experiment had a pulse duration of 600 ns and an amplitude of 16.2 kV/cm. Pulse shapes are nearly identical in each solution tested (Fig. 1). For experiments with calcium buffer introduction by perfusion, a 35-mm culture dish stage (World Precision Instruments, Sarasota, FL) and a perfusion system with VC-8 valve controller from Warner Instruments (Grand Haven, MI) were used to exchange buffers. Flow of calcium-free buffer at  $\sim 1.5$  mL/min was established before and during the initial 270 s of imaging. Pulse exposure

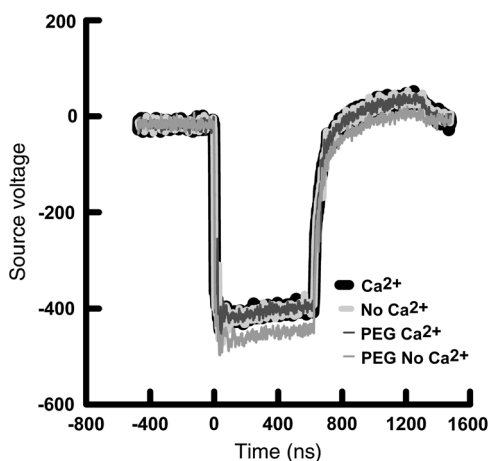


**Fig. 1** Oscilloscope traces of single 600-ns pulses in different solutions: calcium-containing ( $\text{Ca}^{2+}$ ; dark and broad line), calcium-free (No  $\text{Ca}^{2+}$ ; light and broad line), calcium- and PEG-containing (PEG  $\text{Ca}^{2+}$ ; dark and thin line), and calcium-free and PEG-containing (PEG No  $\text{Ca}^{2+}$ ; light and thin line).

was initiated at 240 s, followed by flow of calcium-containing buffer 30 s later. Approximately 60 to 90 s were expected to pass before external calcium concentrations equilibrated around the cells, and it was observed via bleb formation. Average fluorescence intensity was measured for the whole cell within the field of view using ImageJ software.<sup>51</sup> Data were plotted using Grapher 7 (Golden Software, Golden, Colorado) software.

### 3 Results

#### 3.1 Calcium Influx Following Nanosecond Pulsed Electric Field Exposure

To confirm the influx of calcium ions into the cell, the cells were preloaded with CaGr and its fluorescent intensity was monitored before and after nsPEF exposure. Figure 2(a) shows CaGr for 1 and 20 pulse exposures at the time of the pulsing (about 5 s) and for 25 s afterward. The influx of calcium into the cell is presumed to be through pores formed within the plasma membrane.<sup>52–54</sup> Figure 2(b) shows that 1 and 20 pulse exposures cause substantial increase in intracellular calcium. Sham exposed cells show no increase in fluorescent signal over 30 s with a slight reduction due to photobleaching. In the absence of extracellular calcium, the slight increases seen in fluorescence intensity within the cell are likely due to intracellular release from organelles as observed by previous groups.<sup>1,15,55–57</sup> No difference in the means was seen in the peak fluorescence for 1 and 20 nsPEF with extracellular calcium, indicating that both exposures will cause a similar increase in intracellular calcium concentration. This may be an artifact arising from a saturation of the CaGr response.<sup>58</sup> In contrast, increasing numbers of nsPEF have been shown to result in increased thallium ion ( $\text{Tl}^{+}$ ) influx to GH3 (rat pituitary) cells,<sup>50</sup> and higher external  $\text{Ca}^{2+}$  concentrations correlate to lower 50% lethal dose values for Jurkat clone-E6 (human T-lymphocyte) cells.<sup>59</sup> Thus, the case may be that 20 nsPEF cause more or larger membrane pores than 1 nsPEF and let in more than the upper limit of  $\text{Ca}^{2+}$  detection by CaGr. Still, the data presented in Fig. 2 verify that the calcium concentrations increase in the cell postexposure, which could elicit a host of effects, including rapid vesicle-mediated repair, as observed in response to other stressors (e.g., chemical, thermal, etc.) previously investigated.<sup>48,60</sup>

#### 3.2 Measurement of Pore Size

Both 1- and 20-pulse exposures cause an influx of extracellular calcium, but it is unlikely that the damage imposed on the plasma membrane is the same. To differentiate between the degrees of membrane damage inflicted by 1 and 20 pulses, propidium uptake, accepted for identifying plasma membrane electroporation, was used. Figure 3(a) shows representative images of cells before and 120 s after a 20-pulse exposure. These images show that in both the absence and presence of extracellular calcium, propidium influx was observed following 20 pulses. A time trace of the average change in fluorescence intensity of 12–15 cells exposed to either 1 or 20 pulses is shown in Fig. 3(b). The trace indicates that the nearly immediate uptake of propidium occurs after 20 pulses, but is not seen after single-pulse exposures. The concentration of PI was nearly five times in excess of that which is necessary in the exposure buffer to ensure that a small uptake of propidium would be measured. Figure 3(c) shows mean peak (after 120 s) fluorescence in

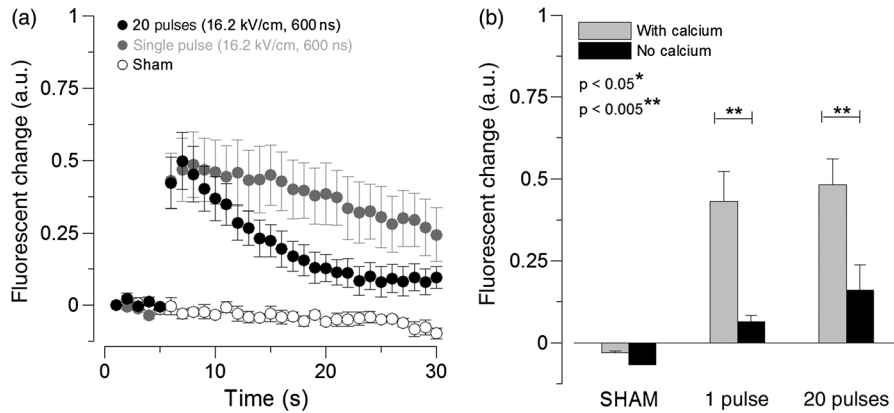


**Fig. 2** (a) Time trace of change in fluorescence intensity of Calcium Green-1 AM ester for cells exposed at 16.2 kV/cm to 1 or 20, 600-ns pulses and sham exposed. (b) Data points represent the average change in fluorescence intensity of 12–15 cells per exposure; error bars represent the standard error of the mean.

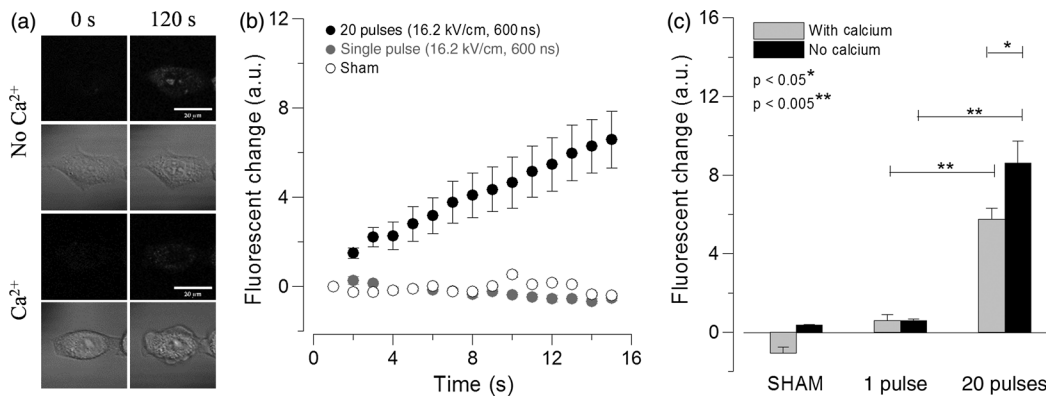


**Fig. 3** (a) Confocal fluorescence and corresponding differential interference contrast (DIC) images of CHO-K1 cells with propidium iodide exposed to 20 pulses (pulse delivered at 5 s) at 16.2 kV/cm in either calcium-containing or calcium-free outside solutions. (b) Time trace of change in fluorescence intensity of propidium for cells exposed at 16.2 kV/cm with either 1 or 20 pulses and sham exposed. (c) Bars indicate peak fluorescence intensity after 120 s. Data represent mean  $\pm$  standard error of 12–15 cells per exposure.

12–15 cells per exposure data point. These data show that the 20-pulse exposure likely opens large holes in the membrane resulting in uptake of propidium, whereas single pulses, which allow unhindered uptake of calcium, remain too small to allow passage of propidium ions (size  $\sim$ 2 nm).<sup>61</sup> These data also show that in the absence of extracellular calcium, with 20 pulses there is a greater influx of propidium into the cell. The reason for this difference is unclear, but suggests that the presence of calcium may affect either pore diameter or number of pores formed in the plasma membrane. It is possible that the presence of calcium changes the morphodynamics<sup>62</sup> and chemistry<sup>56,63,64</sup> of the plasma membrane making it less vulnerable to formation of large ( $>$ 2 nm) pores. Alternatively, calcium may impair propidium ion diffusion by increasing swelling volume and causing more intracellular disorder, or by displacement and increased disruption of the nucleus.

### 3.3 Changes in Plasma Membrane Structure

FM1-43 has been traditionally used to image the process of exocytosis and endocytosis of membrane bound vesicles.<sup>65</sup>

Specifically, FM1-43 dye integrates into the outer layer of phospholipid membranes and dramatically increases its fluorescent quantum yield. Once a cell is stimulated and a vesicle fuses to the plasma membrane, the luminal membrane causes additional integration of FM1-43 dye and thus increased fluorescence signal. When the vesicle membrane is recaptured by endocytosis, the FM dye will be positioned inside the cell. Upon a second stimulation, these dyed vesicles will undergo exocytosis and be expelled from the cell.<sup>66</sup> In addition to tracking endo- and exocytosis, previous researchers have shown that the disruption of the plasma membrane can be observed using FM1-43.<sup>67–69</sup> Traditionally, disruption of the plasma membrane has been observed using Annexin V-FITC to track translocation of phosphatidylserine flipping. Nano-second pulse exposure has been shown to cause rapid increase in FM1-43 fluorescence and specific binding of Annexin V-FITC shortly after exposure (30 s), which strongly suggests that nsPEF exposure causes dramatic and acute changes in membrane asymmetry.<sup>13,70</sup>

The integration, absorption, and exocytosis of vesicles within the cell in the presence and absence of calcium ions are tracked

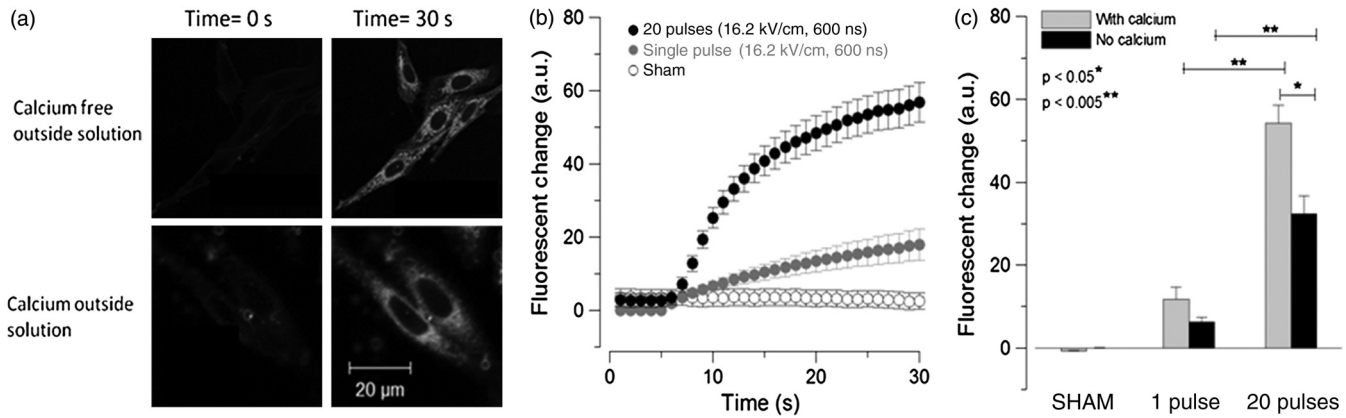


**Fig. 4** (a) CHO-K1 cells with FM1-43 exposed to 20 pulses (pulse delivered at 5 sec) at 16.2 kV/cm in either calcium-containing or calcium-free outside solutions. (b) Time trace of change in fluorescence intensity of FM1-43 for cells exposed at 16.2 kV/cm to 1 or 20 pulses and for sham exposed. (c) Peak fluorescence intensity for each exposure. Data represent mean  $\pm$  standard error of 12–15 cells.

herein using FM1-43 dye. FM1-43 fluorescence increases dramatically upon stimulation by both 1 and 20 nsPEF. Figure 4(a) shows representative images of FM1-43 intensity in CHO-K1 cells before and after receiving 20 pulses; intensity increases in both the presence and absence of calcium in the outside solution. This suggests that the changes in membrane asymmetry brought on by nsPEF-induced formation of nanopores occur regardless of the presence or absence of calcium, although the rate or peak magnitude of change at a particular time after pulsing is influenced by the external calcium concentration. This result supports the hypothesis that the formation of nanopores (calcium-independent phenomena) in the plasma membrane causes lateral diffusion of phospholipids from the inner lamina. Figure 4(b) is a time trace of the average fluorescence for 12–15 cells exposed to either 20 pulses, 1 pulse, or sham exposed. FM1-43 intensity increases well above sham for both 1 and 20 pulse exposures. Figure 4(c) shows the resulting data based on the peak fluorescent intensity for each exposure. Statistically, significant differences are seen between 1 and 20 pulses suggesting that more membrane is presented to the external solution following 20 pulses than a single pulse. These data corroborate what has been seen above with an influx of propidium ions. Additionally, a significant difference is seen with and without extracellular calcium. This difference appears to inversely correspond with an influx of propidium ions, and it likely arises from quicker FM1-43 endocytosis in the presence of calcium.<sup>71</sup> It also may be the case that the nsPEF exposure contributes to the increase of FM1-43 intensity in the presence of calcium because exocytosis of intracellular vesicles is occurring. Indeed, disassembly of filamentous cortical actin, a calcium-dependent process<sup>31</sup> that also corresponds to formation of blebs, is a prerequisite to plasma membrane resealing by lysosomal exocytosis.<sup>32,33</sup> This signal would be in addition to fluorescence intensity changes seen from the formation of pores and hypothesized lateral diffusion of inner leaflet phospholipids. Since FM1-43 has an estimated diameter of 1.10 nm at its thickest axial crosssection,<sup>72</sup> it is possible that the FM1-43 molecules are diffusing into the cell through nanopores formed by nsPEF exposure.<sup>68</sup> Similarly to the propidium uptake results, we cannot rule out a direct effect on membrane structure and physiology due to the presence of extracellular calcium. To test these hypotheses, we followed morphological changes, cytoskeleton integrity, and lysosome movement.

### 3.4 Nanosecond Pulsed Electric Field-Induced Changes in Cellular Morphology

Significant morphological changes were observed in cells exposed to 20 nsPEF in the presence of extracellular calcium. Figure 5 shows an example of cells before and after a 20-pulse exposure, first in calcium-free buffer and then with calcium-containing buffer introduced into the chamber. Specifically, extensive membrane blebbing was observed in the cells following nsPEF exposure after calcium-containing buffer perfusion into the imaging chamber had occurred, whereas cells exposed to the same pulse protocol in the absence of calcium appear to swell uniformly. Calcium exerts these dramatic changes in cellular morphology by disrupting the cytoskeleton, particularly the actin-membrane complex, for blebbing.<sup>73,74</sup> Swelling likely occurs by a colloidal osmotic mechanism.<sup>49</sup> High intracellular calcium can trigger necrotic cell death, and other groups have linked extracellular calcium to changes in cell survival following 60- and 10-ns pulses, suggesting that it does play a role in cell survival.<sup>75</sup> Kymographs [Figs. 5(c) and 5(d)] of the pixels designated by the dark lines in the bright field images at 120 s in Figs. 5(a) and 5(b) show morphological changes occurring within 12 s after nsPEF exposure, and drastic changes by blebbing happen within 90 s of starting the perfusion of calcium-containing buffer into the imaging chamber. Other responses shown later (Fig. 7), however, are quite acute, also occurring within 12 s of exposure. We hypothesize that the actin-membrane decoupling leading to blebbing and the other postexposure responses shown here, such as microtubule depolymerization and interruption of lysosome vesicular transport, are interrelated via a spike in localized calcium ion concentration and happen within a short time of one another.

### 3.5 Lysosome Migration

Spikes in intracellular calcium (as observed with nsPEF stimulation above and in previous publications<sup>15,55</sup>) have been shown to initiate exocytosis of lysosomes, which repair the membrane by traveling along microtubules and fusing with the plasma membrane.<sup>24</sup> This mechanism for membrane repair has been demonstrated by direct physical damage to the plasma membrane by a micropipette and millisecond-duration electrical pulses.<sup>30,48</sup> Preceding data within this paper show that the

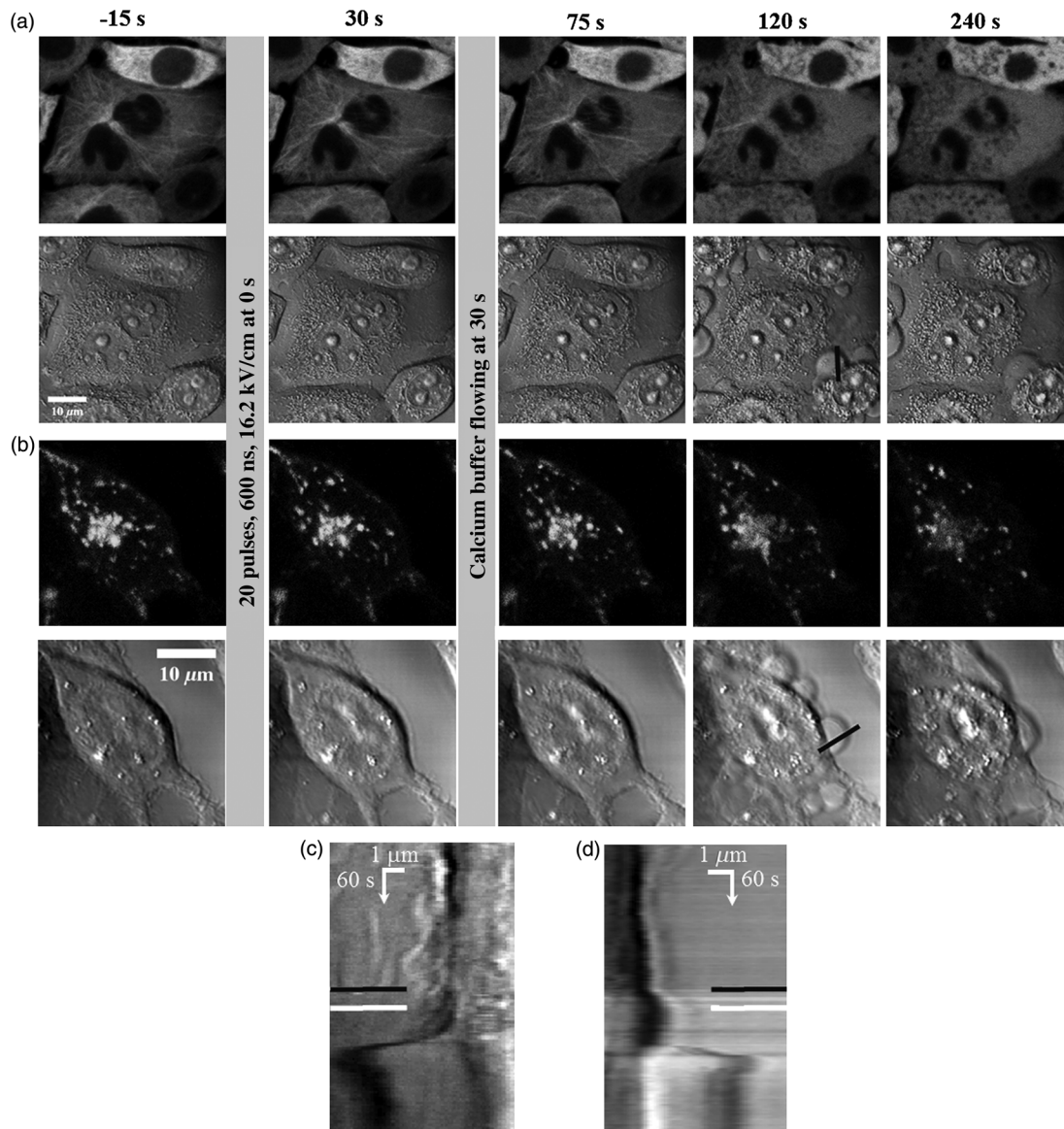


**Fig. 5** Time sequences of confocal fluorescence and DIC images of CHO-K1 (a) mEmerald-tubulin (Video 1) and (b) RFP-LAMP1 (Video 2) cells exposed to 20 pulses (pulse delivered at 0 s) at 16.2 kV/cm in calcium-free buffer, followed by perfusion of calcium-containing buffer beginning at 30 s. In the videos, pulses are delivered at 13 sec and calcium is introduced at 15 s. Kymographs representing the pixels under the dark line in the DIC images for (c) a mEmerald-tubulin cell and (d) a RFP-LAMP1 cell shows swelling after the pulse exposure (dark line) followed by bleb formation within 90 s after calcium buffer introduction (bright line) (Video 1, MOV, 8.81 MB [URL: <http://dx.doi.org/10.1117/1.JBO.19.5.055005.1>]; Video 2, MOV, 1.22 MB [URL: <http://dx.doi.org/10.1117/1.JBO.19.5.055005.2>]; each contains 160 frames at 6 frames per s, with each frame captured every 3 s).

less propidium uptake and greater FM1-43 fluorescence intensity were measured following nsPEF in calcium-containing solution as compared to a calcium-depleted environment, perhaps suggesting membrane repair by exocytosis. For this reason, we chose to track lysosomes specifically using a RFP-LAMP1 CHO-K1 cell line (Fig. 6) to qualitatively monitor the bulk distribution of lysosomes within the cell before and after exposure. Although we are not able to pinpoint the exact movements of the lysosomes in response to the nsPEF due to the rapid 3-D movement of lysosomes, we were able to capture the changes in lysosome distribution within the cell. Example images show that in calcium-containing solution [Fig. 6(a)], there was no observation of lysosomal migration from the perinuclear region (dotted

circles) or to the membrane surface, but rather a stagnation of the natural lysosome migration within the cell. This is apart from any drifting accountable to morphological changes, such as swelling and retraction, which occur. In contrast, within calcium-free solution [Fig. 6(b)], 20 nsPEF cause lysosomes that once were congregated around the nucleus to reallocate to another area of the cell. Notably, some corners of the cells (arrows) already exhibiting dense lysosome presence appear to receive either reinforcement or lose lysosomes after nsPEF exposure, although that does not happen at each corner. Unfortunately, quantification of lysosomal movement remains difficult due to dimensional changes of cells causing shifts in the confocal imaging plane, and while these images are far

from conclusive, they demonstrate that the bulk distribution of lysosomes appears to change following exposure to nsPEF in the absence of calcium.

Stronger evidence of the significance of calcium in relation to lysosomal movement following nsPEF exposure is given by the flow perfusion experiment shown in Fig. 5. The first three-time-point images exhibit changes in positions of the lysosomes at the membrane edges [Fig. 5(b)]. After pulse exposure in the calcium-free buffer, lysosomes continue moving. This motion persists even after flow of the calcium-containing buffer begins 30 s after pulse exposure. Lysosome movement finally ceases approximately 90 s after introduction of calcium, when its external concentration around the cell reaches equilibrium, and bleb formation is observed [Fig. 5(d)]. The dynamics of lysosomal migration is observed more clearly in Video 2. Lysosome movement persists until an influx of calcium occurs, contrasting the general hypotheses that calcium influx induces and that FM1-43 signifies lysosomal exocytosis in response to nsPEF.

### 3.6 Microtubule Disruption

Instead of lysosomal exocytosis, membrane rearrangement may be related to nsPEF-induced breakdown (Fig. 7) of the microtubule cytoskeleton network, which could indicate loss of membrane-to-cytoskeleton attachments and create shear forces that damage plasma and organelle membranes. Microtubules are

the highway for lysosomal traffic,<sup>34–36</sup> and consistent with cessation of lysosome reallocation [Fig. 5(b)], microtubule structure is not altered given exposure to 20 nsPEF in the absence of calcium until an external calcium concentration is established that causes bleb formation [Fig. 5(a) and Video 1]. At this time point, depolymerization of microtubules is rapid and complete. Exposure with 20 pulses does not induce microtubule fragmentation as observed by others at low  $\mu\text{M}$   $\text{Ca}^{2+}$  concentrations,<sup>41,42</sup> but instead elicits rapid microtubule depolymerization or catastrophe.<sup>43,44</sup> High localized concentrations of calcium are known to elicit microtubule fragmentation or depolymerization *in vitro*<sup>43</sup> and *in vivo*.<sup>45</sup> However, the dynamics of microtubule depolymerization with respect to initiation of pulse exposure is unattainable with the delay of external calcium equilibration during the flow perfusion experiments. Therefore, we compared exposure of cells in the presence and absence of calcium in the buffer solution (Fig. 7).

Exposure of CHO-K1 cells with 20 nsPEF in the presence of calcium induces observable depolymerization of microtubules within 10 s [Fig. 7(b)]. Given 20 nsPEF in the absence of calcium, there is still some diminishment of the microtubule network after a longer period [Fig. 7(c)], perhaps because intracellular calcium stores are still released by nsPEF exposure. Unexposed sham cells in calcium-free outside solution reveal that the microtubule networks remain unperturbed and recognizable over the same duration of imaging [Fig. 7(a)], although

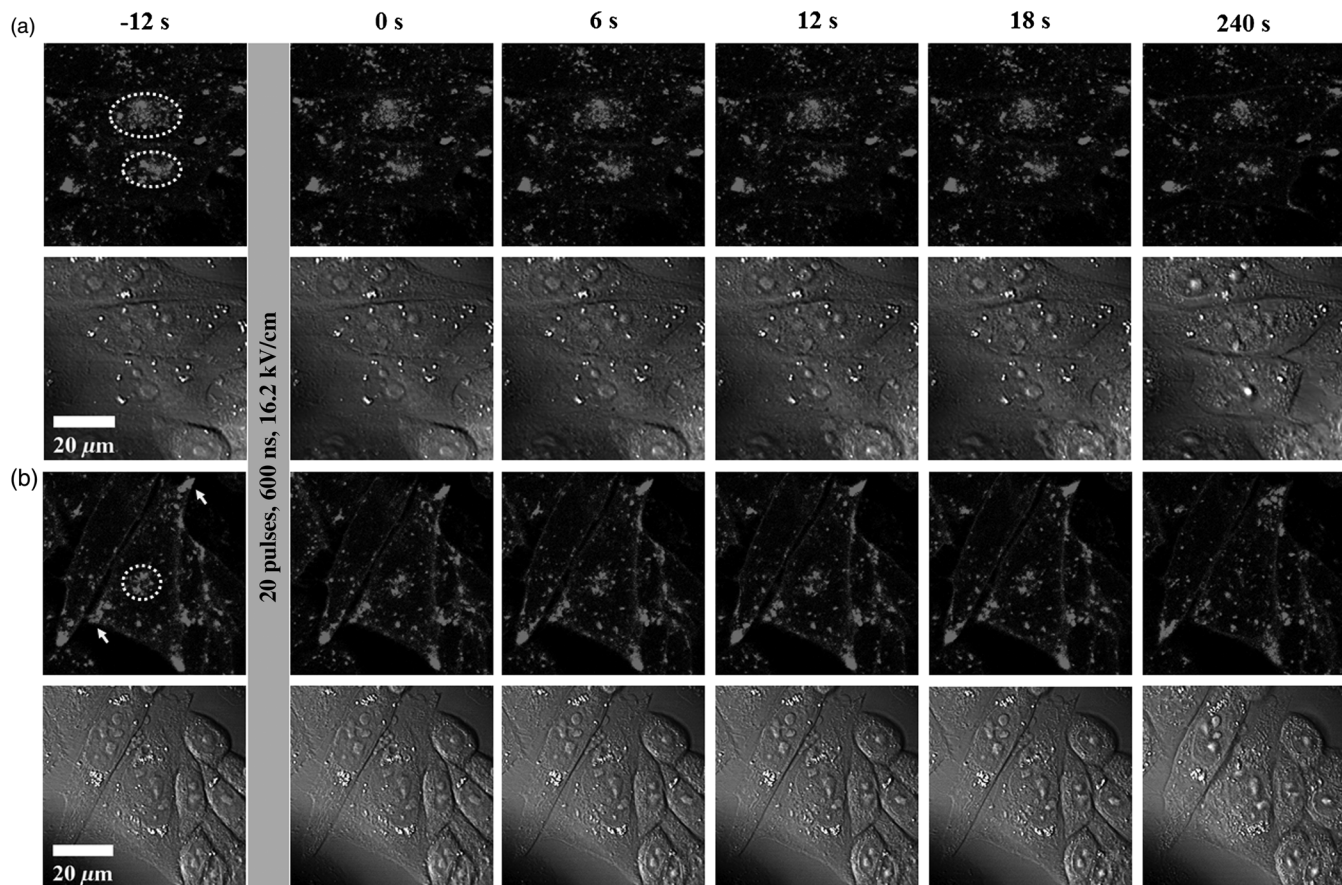


**Fig. 6** Confocal fluorescence (top) and DIC (bottom) images show CHO-K1 cells transfected with RFP-LAMP1 and exposed to 20 pulses (delivery initiated at 0 s) of 16.2 kV/cm and 600-ns duration in the presence (a) and absence (b) of extracellular calcium.

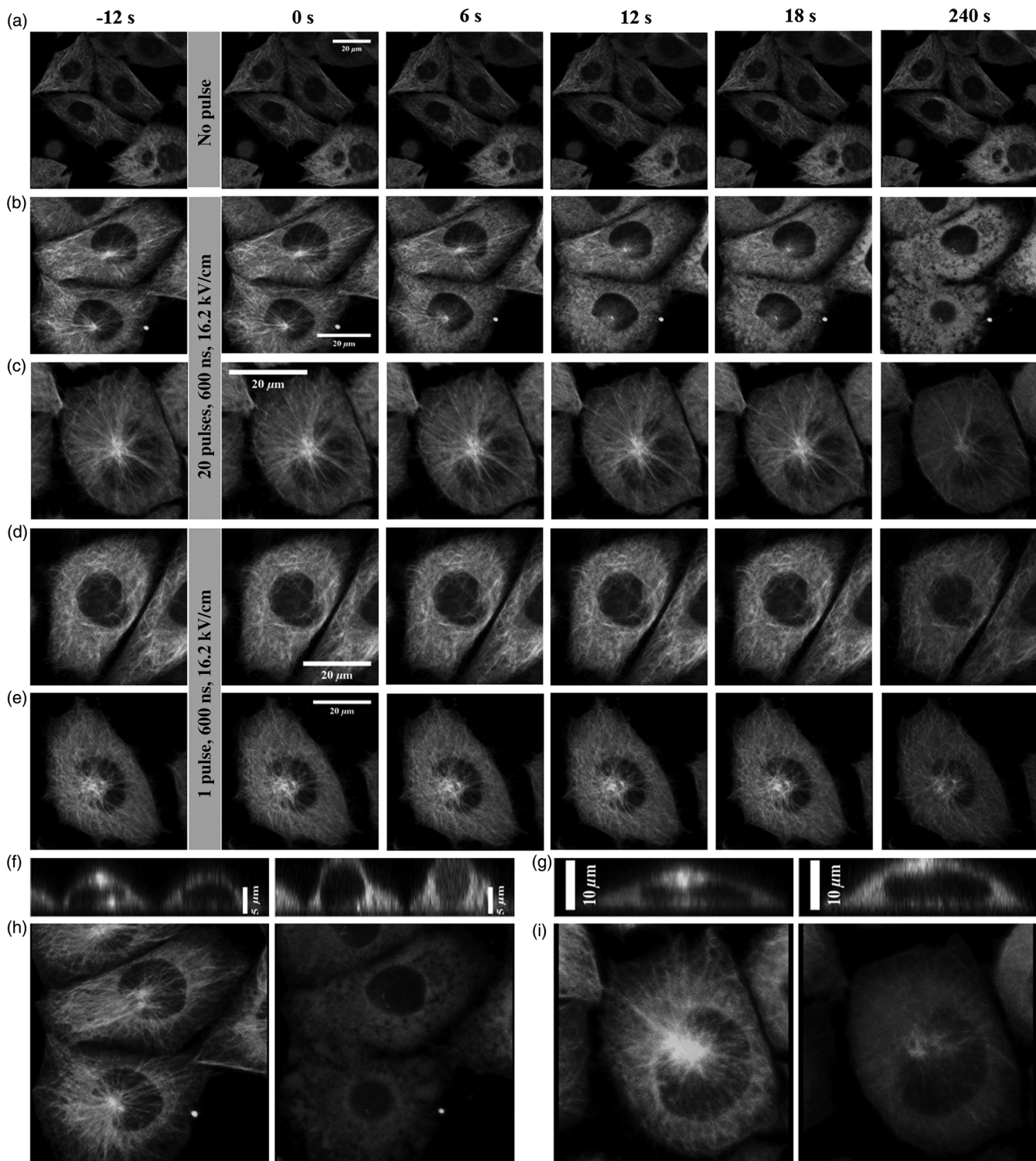


**Fig. 7** Confocal fluorescence images show CHO-K1 cells transfected with mEmerald-tubulin exposed to 0 (a) pulses, 20 (B,C) pulses or 1 (D,E) pulse (delivery initiated at 0 s) of 16.2 kV/cm and 600-ns duration in the presence (b,d) and absence (a,c,e) of extracellular calcium. Cross-sections of Z-stacks through a central location of cells before (left) and after (right) exposure to 20 pulses in the presence (f) and absence (g) of extracellular calcium show swelling in both cases. 3-D projections of brightest points show loss of microtubule structure throughout cell volumes after (right) exposure to 20 pulses in the presence (h) and absence (i) of extracellular calcium.

photobleaching is occurring. With 1 nsPEF in extracellular calcium, some of the microtubules also appear to depolymerize or fragment [Fig. 7(d)], though not to the same extent as with 20 nsPEF, and the observable wavy motion of the microtubules

slows. In calcium-free solution, 1 nsPEF does not appear to alter microtubule behavior [Fig. 7(e)]. These results are consistent with those above using CaGr and FM1-43, which indicate that the membrane damage is greater given 20 nsPEF in calcium

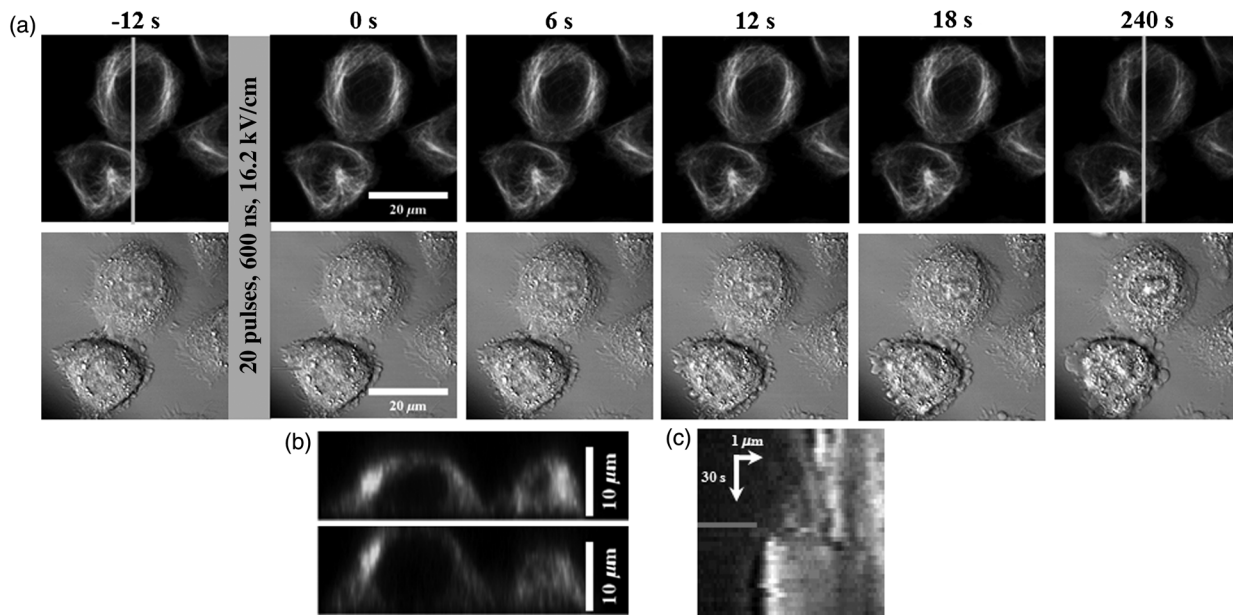


**Fig. 8** (a) Confocal fluorescence (top) and DIC (bottom) images show CHO-K1 cells transfected with mEmerald-tubulin and treated with 1.5 nM paclitaxel for 2 h prior to exposure to 20 pulses (delivery initiated at 0 s) of 16.2 kV/cm and 600-ns duration in the presence of extracellular calcium. (b) Z-stacks through a central location of a cell reveal swelling. (c) (a) kymograph at the position on the cell designated by the dark line in (a) at 0 sec shows bleb formation within 12 s after pulse exposure (dark line).

than for other exposures, and support the hypothesis that larger or more nanopores form following 20 nsPEF. Whether the dominant, causative mechanism of lysosomal stagnation and microtubule disruption is directly calcium-induced<sup>76</sup> or osmotic swelling<sup>77</sup> cannot be determined without further experiments. Therefore, we monitored microtubule integrity during nsPEF

exposure of cells treated with paclitaxel to stabilize microtubules against calcium-induced destabilization and in the presence of PEG to reduce osmotic swelling effects.

Cells exposed to 20 nsPEF in the presence [Fig. 7(f)] and absence [Fig. 7(g)] of extracellular calcium swelled by  $>2\mu\text{m}$  after 4 min, convoluting the direct cause of microtubule

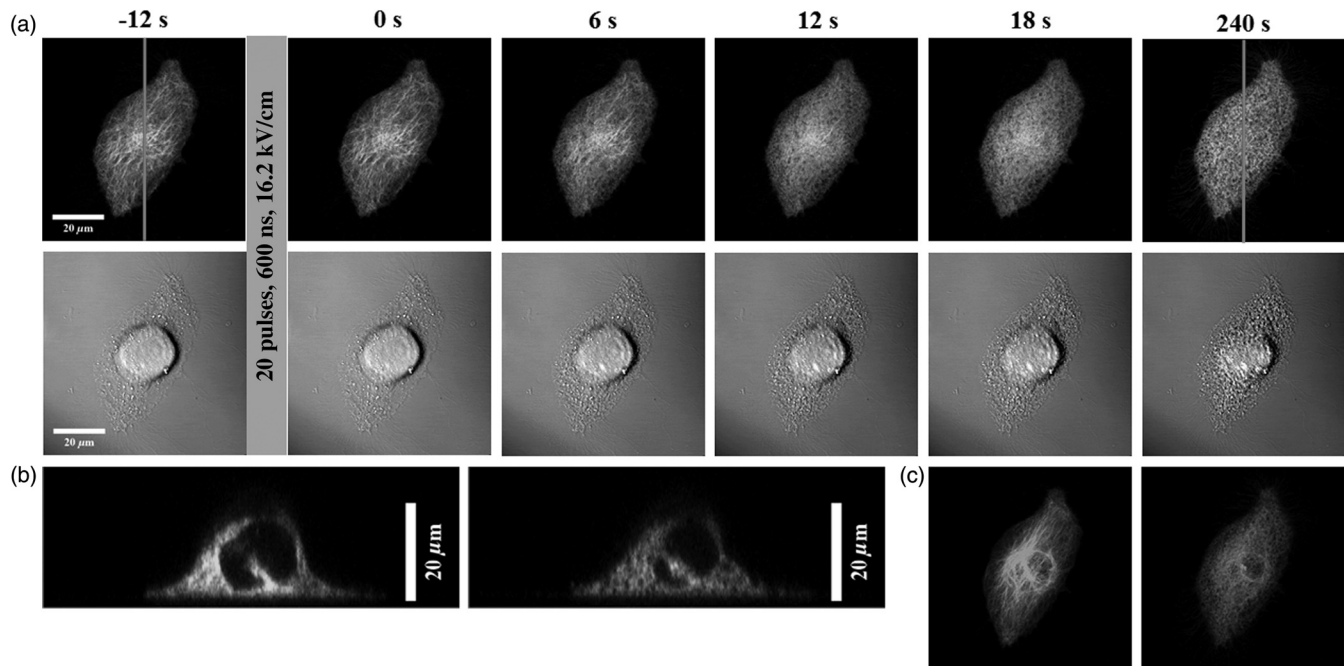


**Fig. 9** (a) Confocal fluorescence (top) and DIC (bottom) images show CHO-K1 cells transfected with mEmerald-tubulin and exposed to 20 pulses (delivery initiated at 0 s) of 16.2 kV/cm and 600-ns duration in presence of extracellular calcium and PEG. (b) Cross-sections of Z-stacks through a central location of a cell show slight shrinkage of the cell after (right) nsPEF exposure. (c) 3-D projections of brightest points before (left) and after (right) exposure to 20 pulses in calcium- and PEG-containing outside solution show loss of microtubule structure throughout the volume of the cell.

depolymerization and lysosome stagnation. Depolymerization does occur and is not an optical artifact, as shown by 3-D projections of brightest points [Figs. 7(h) and 7(i)]. To address whether swelling is the predominant mechanism of microtubule depolymerization, cells were treated with 1.5 nM paclitaxel for 2 h prior to and during exposure to 20 nsPEF in the presence of external calcium (Fig. 8). Paclitaxel is a common drug<sup>78</sup> that induces tubulin polymerization and stabilizes microtubules by binding to the cap,<sup>79,80</sup> which also inhibits calcium interaction with the cap, preventing calcium-induced destabilization.<sup>81</sup> Exposure of paclitaxel-treated cells to 20 nsPEF does not result in microtubule depolymerization [Fig. 8(a)] within the same time frame as for nontreated cells in calcium, while similar morphological changes are seen, including swelling [Fig. 8(b)] and bleb formation [Fig. 8(c)]. Conversely, to reduce swelling and bleb formation but not stabilize microtubules against calcium, cells were exposed to 20 nsPEF in buffer containing calcium and PEG (Fig. 9). Microtubule depolymerization is observed within 10 s, despite a lack of swelling and blebbing. Slight shrinkage and formation of large spaces in the membrane [Fig. 9(b)] preclude absolute conclusions using this average molecular weight of PEG in the buffer during nsPEF exposures. But combined with the results obtained using paclitaxel, this suggests that calcium is the predominant effector of microtubule depolymerization following nsPEF exposure.

## 4 Conclusions

Understanding the cellular impact of nsPEF exposure is fundamental to understanding how cells respond to all electrical stimuli. Electrical pulses create a myriad of effects not seen from other stressors, setting nsPEF apart as a unique and not fully understood stressor. We investigated the extent to which nsPEF, like micro- and millisecond pulses, cause sufficient calcium uptake to perturb intracellular systems responsible for active repair, especially by lysosome exocytosis. We used various staining techniques (CaGr, PI, and FM1-43) to investigate the formation of nanopores in the plasma membrane. Transfected cell lines (RFP-LAMP1 and mEmerald-tubulin) were used to follow potential repair mechanism(s). From the data collected, we can conclude that there appears to be a calcium-dependent phenomenon that elicits membrane rearrangement and microtubule disruption. While data herein neither conclusively points to nor excludes lysosome or vesicle exocytosis as an active repair mechanism following nsPEF exposure in general, it confirms that at a high, threshold nsPEF dosage, lysosome migration halts in the presence of extracellular calcium. Data presented showing influx of extracellular calcium ions into the cell for both single and multiple pulse exposures are not surprising. However, if active cellular repair mechanism(s) are solely triggered by influx of extracellular calcium, one would expect to see a similar repair response to any stimulus (electrical, mechanical, and chemical) that causes acute calcium influx through the plasma membrane. We aim by continuing this work to determine whether the degree of membrane damage is “sensed” by the cell and the resulting repair mechanism(s) are tuned to the degree of insult or whether such response is generic. We believe that using nsPEF to tune the degree of insult acutely and without direct membrane contact enables us to determine if such a distinction occurs. By observing lysosome movement specifically using fluorescent tags, we saw that the microtubule network structure degrades and lysosome movement quickly ceases given 20 pulses of 600-ns PEF in calcium-containing

solution, whereas the distribution of lysosomes within the cell does in fact change following nsPEF exposure in the absence of extracellular calcium. However, further work and a more refined analysis are necessary to quantitate this phenomenon more conclusively. In summary, we believe that nsPEF-induced membrane permeabilization and subsequent calcium ion influx, the extent of which depends on nsPEF dosage, set off a cascade of events that dictate cellular response and may ultimately determine postexposure survival.

## Acknowledgments

The authors would like to thank Dr. Xiao Shu from Old Dominion University for constructing the custom, variable pulse width, and high voltage pulsing system. We wish to thank the Oak Ridge Institute for Science & Education Postdoctoral Research Associateship program and the Air Force Research Laboratory for providing us with the opportunity to conduct this study. This study was supported by a grant from the Air Force Office of Scientific Research (Grant No. AFOSR-LRIR 13RH08COR).

## References

1. K. S. Schoenbach et al., “Bioelectric effects of nanosecond pulses,” *IEEE T. Dielect. El. In.* **14**(5), 1088–1109 (2007).
2. S. Katsuki et al., “Sterilization of bacterial spore using intense nanosecond pulsed electric fields with a pressurized flow system,” in *Proc. IEEE 35th International Conference on Plasma Science*, Karlsruhe, Germany, p. 1, IEEE, New York, NY (2008).
3. R. Nuccitelli et al., “Nanosecond pulsed electric fields cause melanomas to self-destruct,” *Biochem. Biophys. Res. Commun.* **343**(2), 351–360 (2006).
4. R. P. Joshi et al., “Model study of time-dependent muscle response to pulsed electrical stimulation,” *Bioelectromagnetics* **31**(5), 361–370 (2010).
5. R. P. Joshi et al., “Simulation studies of ultrashort, high-intensity electric pulse induced action potential block in whole-animal nerves,” *IEEE T. Bio-Med. Eng.* **55**(4), 1391–1398 (2008).
6. R. Nuccitelli et al., “A new pulsed electric field therapy for melanoma disrupts the tumor’s blood supply and causes complete remission without recurrence,” *Int. J. Cancer* **125**(2), 438–445 (2009).
7. J. Deng et al., “The effects of intense submicrosecond electrical pulses on cells,” *Biophys. J.* **84**(4), 2709–2714 (2003).
8. S. H. Jayaram et al., “Effects of process and product parameters on the shape of nanosecond pulses used in high-field liquid food treatment,” *IEEE T. Ind. Appl.* **41**(2), 520–526 (2005).
9. K. H. Schoenbach, X. Shu, and J. T. Camp, “Subnanosecond electrical pulses for medical therapies and medical imaging,” in *Proc. 2008 IEEE International Power Modulators and High Voltage Conference*, Las Vegas, NE, p. 60, IEEE New York, NY (2008).
10. K. H. Schoenbach et al., “Bioelectrics—new applications for pulsed power technology,” *IEEE T. Plasma. Sci.* **30**(1), 293–300 (2002).
11. A. G. Pakhomov et al., “Membrane permeabilization and cell damage by ultrashort electric field shocks,” *Arch. Biochem. Biophys.* **465**(1), 109–118 (2007).
12. A. G. Pakhomov et al., “Long-lasting plasma membrane permeabilization in mammalian cells by nanosecond pulsed electric field (nsPEF),” *Bioelectromagnetics* **28**, 655–663 (2007).
13. P. T. Vernier et al., “Nanoelectropulse-induced phosphatidylserine translocation,” *Biophys. J.* **86**(6), 4040–4048 (2004).
14. Y. Sun et al., “Fluorescence microscopy imaging of electroperturbation in mammalian cells,” *J. Biomed. Opt.* **11**(2), 024010–024018 (2006).
15. P. T. Vernier et al., “Calcium bursts induced by nanosecond electric pulses,” *Biochem. Biophys. Res. Commun.* **310**(2), 286–295 (2003).
16. W. E. Ford et al., “Nanosecond pulsed electric fields stimulate apoptosis without release of pro-apoptotic factors from mitochondria in B16f10 melanoma,” *Arch. Biochem. Biophys.* **497**(1–2), 82–89 (2010).
17. P. T. Vernier et al., “Ultrashort pulsed electric fields induce membrane phospholipid translocation and caspase activation: differential sensitivities of Jurkat T lymphoblasts and rat glioma C6 cells,” *IEEE T. Dielect. El. In.* **10**(5), 795–809 (2003).

18. S. J. Beebe et al., "Nanosecond, high-intensity pulsed electric fields induce apoptosis in human cells," *FASEB J.* **17**(11), 1493–1495 (2003).
19. S. J. Beebe et al., "Nanosecond pulsed electric field (nsPEF) effects on cells and tissues: apoptosis induction and tumor growth inhibition," *IEEE T. Plasma. Sci.* **30**(1), 286–292 (2002).
20. S. J. Beebe et al., "Diverse effects of nanosecond pulsed electric fields on cells and tissues," *DNA Cell. Biol.* **22**(12), 785–796 (2003).
21. P. L. McNeil and T. Kirchhausen, "An emergency response team for membrane repair," *Nat. Rev. Mol. Cell. Biol.* **6**(6), 499–505 (2005).
22. K. C. Smith and J. C. Weaver, "Active mechanisms are needed to describe cell responses to submicrosecond, megavolt-per-meter pulses: cell models for ultrashort pulses," *Biophys. J.* **95**(4), 1547–1563 (2008).
23. J. C. Weaver, "Electroporation of biological membranes from multicellular to nano scales," *IEEE T. Dielect. El. In.* **10**(5), 754–768 (2003).
24. P. L. McNeil and R. A. Steinhardt, "Loss, restoration, and maintenance of plasma membrane integrity," *J. Cell. Biol.* **137**(1), 1–4 (1997).
25. A. Reddy, E. V. Caler, and N. W. Andrews, "Plasma membrane repair is mediated by Ca<sup>2+</sup>-regulated exocytosis of lysosomes," *Cell* **106**(2), 157–169 (2001).
26. C. Czibener et al., "Ca<sup>2+</sup> and synaptotagmin VII-dependent delivery of lysosomal membrane to nascent phagosomes," *J. Cell. Biol.* **174**(7), 997–1007 (2006).
27. J. K. Jaiswal, N. W. Andrews, and S. M. Simon, "Membrane proximal lysosomes are the major vesicles responsible for calcium-dependent exocytosis in nonsecretory cells," *J. Cell Biol.* **159**(4), 625–635 (2002).
28. N. W. Andrews, "Regulated secretion of conventional lysosomes," *Trends Cell Biol.* **10**(8), 316–321 (2000).
29. E. J. Blott and G. M. Griffiths, "Secretory lysosomes," *Nat. Rev. Mol. Cell Biol.* **3**(2), 122–131 (2002).
30. A. Rodriguez et al., "Lysosomes behave as Ca<sup>2+</sup>-regulated exocytic vesicles in fibroblasts and epithelial cells," *J. Cell Biol.* **137**(1), 93–104 (1997).
31. R. Wollman and T. Meyer, "Coordinated oscillations in cortical actin and Ca<sup>2+</sup> correlate with cycles of vesicle secretion," *Nat. Cell Biol.* **14**(12), 1261–1269 (2012).
32. P. L. McNeil, "Repairing a torn cell surface: make way, lysosomes to the rescue," *J. Cell Sci.* **115**(5), 873–879 (2002).
33. K. Miyake et al., "An actin barrier to resealing," *J. Cell Sci.* **114**(19), 3487–3494 (2001).
34. M. Collot, D. Louvard, and S. J. Singer, "Lysosomes are associated with microtubules and not with intermediate filaments in cultured fibroblasts," *P. Natl. Acad. Sci. U. S. A.* **81**(3), 788–792 (1984).
35. R. Matteoni and T. E. Kreis, "Translocation and clustering of endosomes and lysosomes depends on microtubules," *J. Cell Biol.* **105**(3), 1253–1265 (1987).
36. C. M. Perou and J. Kaplan, "Chediak-Higashi syndrome is not due to a defect in microtubule-based lysosomal mobility," *J. Cell Sci.* **106**(1), 99–107 (1993).
37. J. A. Swanson et al., "Radial movement of lysosomes along microtubules in permeabilized macrophages," *J. Cell Sci.* **103**(1), 201–209 (1992).
38. J. Swanson, E. Burke, and S. C. Silverstein, "Tubular lysosomes accompany stimulated pinocytosis in macrophages," *J. Cell Biol.* **104**(5), 1217–1222 (1987).
39. M. Matsushita et al., "A novel kinesin-like protein, KIF1Bbeta3 is involved in the movement of lysosomes to the cell periphery in non-neuronal cells," *Traffic* **5**(3), 140–151 (2004).
40. R. C. Weisenberg, "Microtubule formation *in vitro* in solutions containing low calcium concentrations," *Science* **177**(4054), 1104–1105 (1972).
41. M. Schliwa, "Microtubule-dependent intracellular transport in chromatophores," in *International Cell Biology 1980–1981*, H. G. Schweiger, Ed., pp. 275–285, Springer, Berlin Heidelberg (1981).
42. W. J. Deery, A. R. Means, and B. R. Brinkley, "Calmodulin-microtubule association in cultured mammalian cells," *J. Cell Biol.* **98**(3), 904–910 (1984).
43. E. T. O'Brien, E. D. Salmon, and H. P. Erickson, "How calcium causes microtubule depolymerization," *Cell Motil. Cytoskeleton* **36**(2), 125–135 (1997).
44. A. Lieuvain et al., "Intrinsic microtubule stability in interphase cells," *J. Cell Biol.* **124**(6), 985–996 (1994).
45. C. Keith et al., "Microinjection of Ca<sup>++</sup>-calmodulin causes a localized depolymerization of microtubules," *J. Cell Biol.* **97**(6), 1918–1924 (1983).
46. D. G. Harkin and E. D. Hay, "Effects of electroporation on the tubulin cytoskeleton and directed migration of corneal fibroblasts cultured within collagen matrices," *Cell Motil. Cytoskeleton* **35**(4), 345–357 (1996).
47. C. Kanthou et al., "The endothelial cytoskeleton as a target of electroporation-based therapies," *Mol. Cancer Ther.* **5**(12), 3145–3152 (2006).
48. C. Huynh et al., "Defective lysosomal exocytosis and plasma membrane repair in Chediak-Higashi/beige cells," *P. Natl. Acad. Sci. U. S. A.* **101**(48), 16795–16800 (2004).
49. O. M. Nesin et al., "Manipulation of cell volume and membrane pore comparison following single cell permeabilization with 60- and 600-ns electric pulses," *Biochim. Biophys. Acta.* **1808**(3), 792–801 (2011).
50. B. L. Ibey et al., "Plasma membrane permeabilization by trains of ultrashort electric pulses," *Bioelectrochemistry* **79**(1), 114–121 (2010).
51. W. S. Rasband, *Image J*, U. S. National Institutes of Health, Bethesda (1997–2009).
52. A. G. Pakhomov and O. N. Pakhomova, "Nanopores: a distinct transmembrane passageway in electroporated cells," in *Advanced Electroporation Techniques in Biology in Medicine*, A. G. Pakhomov, D. Miklavcic, and M. S. Markov, Eds., pp. 177–194, CRC Press, Boca Raton, FL (2010).
53. A. G. Pakhomov et al., "Lipid nanopores can form a stable, ion channel-like conduction pathway in cell membrane," *Biochem. Biophys. Res. Commun.* **385**(2), 181–186 (2009).
54. P. T. Vernier et al., "Nanosecond electric pulse-induced calcium entry into chromaffin cells," *Bioelectrochemistry* **73**(1), 1–4 (2008).
55. H. T. Beier et al., "Resolving the spatial kinetics of electric pulse-induced ion release," *Biochem. Biophys. Res. Commun.* **423**(4), 863–866 (2012).
56. G. P. Tolstykh et al., "Activation of intracellular phosphoinositide signaling after a single 600 nanosecond electric pulse," *Bioelectrochemistry* **94**, 23–29 (2013).
57. I. Semenov, S. Xiao, and A. G. Pakhomov, "Primary pathways of intracellular Ca(2+) mobilization by nanosecond pulsed electric field," *Biochim. Biophys. Acta.* **1828**(3), 981–989 (2013).
58. S. Gilroy and R. L. Jones, "Gibberellic acid and abscisic acid coordinately regulate cytoplasmic calcium and secretory activity in barley aleurone protoplasts," *P. Natl. Acad. Sci. U. S. A.* **89**(8), 3591–3595 (1992).
59. B. L. Ibey et al., "Dose-dependent thresholds of 10-ns electric pulse induced plasma membrane disruption and cytotoxicity in multiple cell lines," *PLoS. One* **6**(1), e15642 (2011).
60. F. W. Chen, C. Li, and Y. A. Ioannou, "Cyclodextrin induces calcium-dependent lysosomal exocytosis," *PLoS. One* **5**(11), e15054 (2010).
61. A. M. Bowman et al., "Analysis of plasma membrane integrity by fluorescent detection of Tl(+) uptake," *J. Membr. Biol.* **236**(1), 15–26 (2010).
62. I. Levental et al., "Calcium-dependent lateral organization in phosphatidylinositol 4,5-bisphosphate (PIP<sub>2</sub>)- and cholesterol-containing monolayers," *Biochemistry* **48**(34), 8241–8248 (2009).
63. P. T. Vernier et al., "Electroporating fields target oxidatively damaged areas in the cell membrane," *PLoS. One* **4**(11), e7966 (2009).
64. G. P. Tolstykh et al., "600 ns pulse electric field-induced phosphatidylinositol-bisphosphate depletion," *Bioelectrochemistry* (2014).
65. A. W. Henkel, J. Lübke, and W. J. Betz, "FM1-43 dye ultrastructural localization in and release from frog motor nerve terminals," *P. Natl. Acad. Sci. U. S. A.* **93**(5), 1918–1923 (1996).
66. M. A. Gaffield and W. J. Betz, "Imaging synaptic vesicle exocytosis and endocytosis with FM dyes," *Nat. Protoc.* **1**(6), 2916–2921 (2007).
67. A. Zweifach, "FM1-43 reports plasma membrane phospholipid scrambling in T-lymphocytes," *Biochem. J.* **349**(1), 255–260 (2000).
68. R. L. Vincelette et al., "Thresholds for phosphatidylserine externalization in chinese hamster ovarian cells following exposure to nanosecond pulsed electrical fields (nsPEF)," *PLoS. One* **8**(4), e63122 (2013).
69. J. M. Escoffre et al., "Membrane disorder and phospholipid scrambling in electroporated and viable cells," *Biochim. Biophys. Acta.* **1838**(7), 1701–1709 (2014).
70. P. T. Vernier et al., "Nanopore formation and phosphatidylserine externalization in a phospholipid bilayer at high transmembrane potential," *J. Am. Chem. Soc.* **128**(19), 6288–6289 (2006).
71. *FM Lipophilic Styryl Dyes*, Molecular Probes, Inc., Eugene, OR, [tools.lifetechnologies.com/content/sfs/manuals/mp34653.pdf](http://tools.lifetechnologies.com/content/sfs/manuals/mp34653.pdf) (2005).

72. Y. Wu et al., "Permeation of styryl dyes through nanometer-scale pores in membranes," *Biochemistry* **50**(35), 7493–7502 (2011).
73. M. P. Sheetz, J. E. Sable, and H. G. Dobereiner, "Continuous membrane-cytoskeleton adhesion requires continuous accommodation to lipid and cytoskeleton dynamics," *Annu. Rev. Biophys. Biomol. Struct.* **35**, 417–434 (2006).
74. M. A. Rassokhin and A. G. Pakhomov, "Electric field exposure triggers and guides formation of pseudopod-like blebs in U937 monocytes," *J. Membr. Biol.* **245**(9), 521–529 (2012).
75. W. H. Baldwin et al., "Membrane permeability and cell survival after nanosecond pulsed-electric-field exposure: significance of exposure-media composition," *IEEE T. Plasma. Sci.* **38**(10), 2948–2953 (2010).
76. A. R. Prescott et al., "Effects of elevated intracellular magnesium on cytoskeletal integrity," *J. Cell Sci.* **89**(3), 321–329 (1988).
77. O. M. Nesin et al., "Manipulation of cell volume and membrane pore comparison following single cell permeabilization with 60- and 600-ns electric pulses," *Biochim. Biophys. Acta.* **1808**(3), 792–801 (2011).
78. M. A. Jordan and L. Wilson, "Microtubules as a target for anticancer drugs," *Nat. Rev. Cancer* **4**(4), 253–265 (2004).
79. H. Xiao et al., "Insights into the mechanism of microtubule stabilization by Taxol," *P. Natl. Acad. Sci. U. S. A.* **103**(27), 10166–10173 (2006).
80. L. A. Amos and J. Lowe, "How taxol stabilises microtubule structure," *Chem. Biol.* **6**(3), R65–R69 (1999).
81. P. B. Schiff, J. Fant, and S. B. Horwitz, "Promotion of microtubule assembly *in vitro* by taxol," *Nature* **277**(5698), 665–667 (1979).

**Gary Lee Thompson** received his BS degree in chemical engineering in 2004 from the University of South Carolina and a PhD degree in bioengineering in 2011 from Clemson University. He is currently an Oak Ridge Institute for Science & Education postdoctoral research associate at the Tri-Service Research Laboratory in San Antonio, Texas. His current research interests include advanced nanoscopy techniques, electromechanical coupling in biomolecules, mechanobiology of

cellular responses to electrical stimulation, and biophysical mechanisms underlying electroporation.

**Caleb C. Roth** is a PhD degree candidate in the radiation biology program, school of medicine, from the University of Texas Health Science Center San Antonio in the laboratory of Randolph Glickman. He is a SMART/ASEE scholar, Cohort 2012, sponsored by the Air Force Research Laboratory 711th HPW. He has worked as a contractor for the US Air Force for 10 years and studies the biophysical properties of mammalian cells exposed to nanosecond pulsed electrical fields.

**Danielle R. Dalzell** received her BS degree in chemistry from the University of Colorado in 2008. Upon graduation, she worked for the Air Force Research Laboratory 711th HPW with a research focus on the bioeffects of mammalian cells exposed to nanosecond pulsed electric fields. She is currently a captain in the United States Air Force and will be pursuing a MS degree in biochemistry.

**Marjorie Kuipers** received her BS degree in cellular and molecular biology from the University of Michigan in 2002, an MS degree in toxicology from the University of Florida in 2007, and a PhD degree in biology from Florida State University in 2010. She is currently pursuing a DVM from the University of Florida with a public health interest in animal and agricultural production in the China and Persian Gulf regions.

**Bennett L. Ibey** is a senior research biomedical engineer with the 711th human performance wing of the Air Force Research Laboratory, Radio Frequency Bioeffects Branch. He received a PhD degree in biomedical engineering from Texas A&M University in 2006 with a focus on biomedical optics. Since that time, his research interests have focused on the interaction between tissue and nanosecond pulsed electric fields and high peak power microwave bioeffects.